Theory and simulations for hard-disk models of binary mixtures of molecules with internal degrees of freedom

Fraser, Diane P.; Zuckermann, Martin J.; Mouritsen, Ole G.

Published in:
Physical Review A

Link to article, DOI:
10.1103/PhysRevA.43.6642

Publication date:
1991

Document Version
Publisher's PDF, also known as Version of record

Theory and simulations for hard-disk models of binary mixtures of molecules with internal degrees of freedom

Diane P. Fraser and Martin J. Zuckermann
Department of Physics and Centre for the Physics of Materials, McGill University, 3600 University Street, Montréal, Québec, Canada H3A 2T8

Ole G. Mouritsen
Department of Structural Properties of Materials, The Technical University of Denmark, Building 307, DK-2800 Lyngby, Denmark

(Received 18 September 1990; revised manuscript received 27 December 1990)

A two-dimensional Monte Carlo simulation method based on the NpT ensemble and the Voronoi tesselation, which was previously developed for single-species hard-disk systems, is extended, along with a version of scaled-particle theory, to many-component mixtures. These systems are unusual in the sense that their composition is not fixed, but rather determined by a set of internal degeneracies assigned to the differently sized hard disks, where the larger disks have the higher degeneracies. Such systems are models of monolayers of molecules with internal degrees of freedom. The combined set of translational and internal degrees of freedom leads to a rich phase structure that includes solid-liquid transitions (governed by the translational variables) as well as transitions involving changes in average disk size (governed by the internal variables). The relationship between these two types of transitions is studied by the method in the case of a binary mixture, and results are presented for varying disk-size ratios and degeneracies. The results are also compared with the predictions of the extended scaled-particle theory. Applications of the model are discussed in relation to lipid monolayers spread on air-water interfaces, and it is concluded, by comparison with experiments, that the hard-disk mixture is an excellent candidate for a minimal model of lipid-monolayer phase behavior.

I. INTRODUCTION

Fluids consisting of multicomponent mixtures of atoms, molecules, or particles are not easy systems to study. For two-dimensional fluids, early theoretical work concentrated on attempting to predict the behavior of single- and multicomponent systems of hard disks using scaled-particle theory (SPT) (Refs. 1–4) and integral-equation techniques.[5–7] Although there exists a plethora of work in three dimensions, fewer systems have been studied in two-dimensions. Extensions to SPT and other integral-equation theories have been made, though, for single- and multicomponent systems of anisotropic particles with hard-core and soft interactions.[8–15] More recently, studies have been concerned with systems in which the composition is not fixed, but is allowed to vary.[16–21] A typical example of variable polydispersity is in the study of nonionic micelles formed by surfactant in water, since theoretical and experimental studies indicate that these micelles are likely to be polydisperse in size[22] with the degree of polydispersity determined by factors such as head-group repulsion, bound water associated with the head groups and the isomeric state of the hydrocarbon chains, as well as surfactant concentration and temperature. A knowledge of the functional form of the low-density, *underlying* distribution allows the behavior of the system to be determined and this behavior is found to be in agreement with simulation results. It is also found that, for small degrees of polydispersity, the thermodynamics of the fluid is well understood in terms of an effective monodisperse fluid.[18] But what if the distribution cannot be expressed in functional form? A typical example of this situation is that of lipid monolayers spread on air-water interfaces in which the "particle" under consideration is a hydrocarbon chain consisting of, say, 14–22 CH_2 units. The study of lipid monolayers is important, since they are models of biological membranes.[23,24] They may be thought of as pseudo-two-dimensional systems of molecules with positional (lateral) as well as acyl-chain conformation degrees of freedom. These degrees of freedom and the couplings between them impart the monolayer with a rich phase behavior, including the possibility of condensation in one or both sets of variables, sepatately or simultaneously. These complications are reflected in the considerable difficulties encountered in constructing realistic theoretical models of lipid-monolayer phase behavior. The basic problem is that, when both sets of degrees of freedom and their interactions are modeled as realistically as possible,[25–27] it is difficult to make calculations in the transition region. Therefore, the most successful theoretical studies of monolayer phase behavior to date have been based on lattice models which represent the acyl-chain conformational variables accurately, but treat the lateral degrees of freedom approximately via coarse-grained crystalline variables (for example, Potts variables).[28,29]

The other approach is to emphasize the volume exclusion interactions of the system and to approximate the chain conformations. The pseudo-two-dimensional nature of these systems invites the projection of the lipid matrix onto the plane of the monolayer as a first approximation. It is this two-dimensional system that is then studied. The method of projection used determines how good the approximation is. The distribution of chain conformations is polydisperse and continuously variable. But the chains are too short for long-chain polymer approximations to be applicable,[30] and yet are too long for all the conformations to be included both easily and accurately.[31] Attempts at averaging the many conformations into discrete sets of states were first made in the late 1970s. Scott and Cheng[16] considered multistate models in which the number of states [for example, seven for dipalmitoylphosphatidylcholine (DPPC)] varied with the length of the acyl chains. The lipid molecules (as opposed to individual chains) were modeled as hard cylinders with radii determined by the number of gauche rotations in the lipid chains. Chain conformations were grouped according to their cross-sectional area, and statistical weights were assigned using combinatorial arguments. Projecting this system of hard cylinders onto the two-dimensional plane produces a system of polydisperse hard disks. Scaled-particle theory for hard-disk mixtures (SPTM) was then used to model the effects of steric interactions. This was combined with an additional long-range attractive interaction to model the van der Waals forces, and also with the internal rotational energy of the chains. The composition of the system was determined by minimizing the free energy at fixed temperature and area. The interaction strength was varied to fit the transition temperatures for various chain lengths, and results for the transition enthalpies agreed well with experiment. The method allowed extensions to study mixtures of lipids.[16] The seven-state system of Scott and Cheng was also used by Fraser *et al.* in Monte Carlo simulations to examine in-plane orientational ordering of the DPPC molecules. To reflect the asymmetric nature of the molecules, hard-core triatomic molecules with variable bond lengths were used instead of disks.

A simpler approximation was made by Doniach,[32] who considered just two conformational states: one ground state representing the all-*trans* conformation of the acyl chain, which is dominant in the condensed, *gel* phase, and one excited state representing all of the disordered conformations, which are dominant in the *fluid* phase. As with the model of Scott, an internal rotational energy, representing several gauche rotations in the acyl chain, was assigned to the excited state as well as a high effective weight or degeneracy. The ground state has zero internal energy and is nondegenerate. By assigning different cross-sectional areas and average nematic orders to the states, according to the average conformations of the chains, and formulating nearest-neighbor interactions in terms of these variables, the model allows different interactions between neighboring chains in different states. These interactions represent both dispersion forces and steric interactions. Doniach showed that this model is isotropic to a nearest-neighbor Ising model with a temperature-dependent external field $H(T) \propto (T_1 - T)$. The transformed model is therefore a simple model for first-order phase transitions provided that $T_1 < T_c$, where T_c is the critical temperature of the zero-field Ising model. The model is directly applicable to lipid monolayers when an external lateral pressure Π is included in the formalism,[33] and again exhibits a first-order phase transition at lateral pressures below the critical pressure. The Doniach model has been studied using both mean-field theory and computer simulations and has been extended to include eight "intermediate" conformational states by Pink *et al.*[34] and all possible conformational states by Tevlin *et al.*[31,35,36] The problem with these models is that they are lattice models that describe the principal phase transitions in terms of configurational entropy and internal energy. However, in both lipid monolayers and bilayers, the phase transition under consideration is a transition between a fluid and a solid phase and therefore involves additional translational degrees of freedom. Similarly, the conformational models of Scott, which are based on SPT, can only be used to describe fluid phases.

In this paper we present studies of binary mixtures of disks in which the composition is allowed to vary with density and pressure according to preset degeneracies. Since the degeneracies can be written in terms of internal free energies of the disks, this system, with suitable choice of parameters, can be considered as a minimal model of a lipid monolayer. As such, it can be described as a noninteracting Doniach model in which the two conformational states are replaced by interconvertable hard disks. The larger of the two disk sizes corresponds to the excited, conformationally disordered acyl-chain state and the small disk size corresponds to all-*trans* state. The advantage of this model is that it exhibits both fluid and solid phases in a natural manner. In a previous paper[37] (hereafter referred to as I) we presented the results from constant NpT Monte Carlo simulations of two-dimensional hard-disk systems which used a new technique, based on the Voronoi tesselation[38] of the system, to keep track of nearest neighbors. it was shown how an analysis of the Voronoi tesselation can be used to isolate the liquid-solid transition in single-species hard-disk systems. This analysis is based on the edge-length distribution function of the Voronoi polygons. A particular decomposition of this distribution function provides a strong signal of the liquid-solid transition that is superior to the signal seen in the pressure-area (p-A) isotherm. The same analysis, applied here to the binary mixtures, is shown to reveal the liquid-solid phase transition of the mixtures and the transition from large disks to small disks with increasing pressure, which, for convenience, we shall refer to as the "large-small" transition. It is important to note that this large-small transition is not a phase transition but rather a continuous change in the relative concentrations of the two disk sizes. The binary mixtures studied can be described by two independent parameters. The first is the ratio of large-disk to small-disk diameters, $\chi = (\sigma_1/\sigma_2)$, and the second is the ratio of the degeneracies, $\nu = (D_1/D_2)$. By changing these two parameters it is possible to change the range of densities over which the large-small transition takes place, that is,

the position of this transition relative to the liquid-solid transition, and the sharpness of the transition.

For comparison with the computer-simulation results we present a theoretical analysis of this hard-disk binary fluid based on the scaled-particle theory. This is similar to the SPTM analysis of Scott and Cheng[16] but without interparticle interactions. The SPTM has been extended to include the degeneracy of the disks and a derivation of this extension (SPTD) will be given in Sec. III. The SPTD equation is used to predict the position and sharpness of the large-small transition. Comparisons with constant NpT Monte Carlo simulations show excellent agreement in the liquid phase for all systems studied. The SPTD predictions for the concentration-density profiles are also excellent through the liquid-solid transition and into the solid phase for all but a few systems. The few systems that show deviations from the SPTD profile through the liquid-solid transition region show agreement again at higher densities. As with all theoretical equations of state, the compressibility factor (reduced pressure) $\varphi=p/\rho kT$ as determined by the SPTD equation diverges from the simulation data at the onset of the liquid-solid packing transition.

For high degeneracies and large size ratios the p-A isotherms for the SPTD equation reflect, visibly, the large-small transition. By selecting degeneracies and size ratios for the Monte Carlo simulations such that the large-small transition is coincident with the liquid-solid transition, the liquid-solid packing transition can be used to accentuate the large-small tansition. It can be argued that, although the two transitions can be made coincident, such that the system will contain predominantly large disks at densities below the combined transition and small disks above the combined transition, the system will not go directly from a large-disk liquid to a small-disk solid. The effects of the packing of the disks allow domains of large-disk solid and of small-disk liquid within the transition region. The effects of packing are also seen to account for the aforementioned deviations from SPTD of the concentration-density profile across the liquid-solid transtion.

II. HARD-DISK MIXTURES

The simplest two-dimensional hard-disk system is that consisting of a single size of particle. The hard-core nature of the interaction potential gives a single equation of state

$$\frac{p}{\rho kT}=\varphi(\rho)\ , \tag{1}$$

where $\varphi(\rho)$ is some function of density ρ, only.

The equation of state of a hard-core mixture of s species will depend upon the concentrations, $\underline{n}=\{n_1,n_2,\ldots,n_s\}$, and relative sizes, $\underline{\sigma}=\{\sigma_1,\sigma_2,\ldots,\sigma_s\}$, of the different species present.

For this system Eq. (1) must be modified such that $\varphi=\varphi(\rho,\underline{n},\underline{\sigma})$. For a binary mixture we have $s=2$ with $n_1+n_2=1$. $\varphi(\rho,\underline{n},\underline{\sigma})$ then reduces to $\varphi(\rho,n_1,\sigma_1/\sigma_2)$.

An extension of the hard-disk mixture is to allow the concentrations of the species to vary with density. This is achieved by assigning a *degeneracy* D to each species. The degeneracy of species i, D_i, can be related to an internal free energy $V_{\rm int}(i)$ such that

$$D_i\propto e^{-V_{\rm int}(i)/kT}\ , \tag{2}$$

where T is the temperature and k is Boltzmann's constant. If the concentrations $\underline{n}$ vary only with density, the disk sizes, and the degeneracies $\underline{D}=\{D_1,D_2,\ldots,D_s\}$, then for a binary mixture we can write

$$\frac{p}{\rho kT}=\varphi(\rho,\chi,\nu)\ , \tag{3}$$

where $\chi=\sigma_1/\sigma_2$ and $\nu=D_1/D_2$. In other words, there should be a single equation of state for given values of χ and ν. If, however, the systems exhibit metastability, there are likely to be hysteresis effects.

III. SCALED-PARTICLE THEORY

In the scaled-particle formalism, the chemical potential and pressure of a system are determined by considering the work done to insert a *scaled particle*[39] into the system. For a mixture of hard disks the SPT chemical potential and equation of state are[2] (SPTM)

$$\frac{\mu_i}{kT}=\ln\rho_i\Lambda_i^2-\ln(1-\eta)+\frac{\pi}{2}\frac{\sigma_i\sum_j\rho_j\sigma_j}{1-\eta}+\frac{\pi}{4}\frac{p}{kT}\sigma_i^2\ , \tag{4}$$

with

$$\frac{p}{\rho kT}=\frac{1}{1-\eta}+\frac{\pi}{4\rho}\frac{(\sum_i\rho_i\sigma_i)^2}{(1-\eta)^2}\ , \tag{5}$$

where $\eta=(\pi/4)\sum_i\rho_i\sigma_i^2$ is the packing fraction of the system, μ_i is the chemical potential of species i, and Λ_i^2 is the ideal-gas partition function.

The chemical potential μ_i of species i can be written

$$\mu_i=kT\ln\rho_i\Lambda_i^2+W_i\ , \tag{6}$$

where W_i is the nonideal-gas part of the chemical potential. Suppose that at low density there is a distribution of sizes $u_i(\sigma_i)$, which depends upon the internal energy of the particles, $V_{\rm int}(i)$. The degeneracies D_i are defined by

$$u_i=\frac{D_i}{\sum_j D_j}=C\exp[-\beta V_{\rm int}(i)]\ , \tag{7}$$

which gives

$$\beta V_{\rm int}(i)=\ln C-\ln u_i\ , \tag{8}$$

with $\beta=(kT)^{-1}$ and normalization constant C. The nonideal part of the chemical potential is now

$$\beta W_i=-\ln(1-\eta)+\frac{\pi}{2}\frac{\sigma_i\sum_j\rho_j\sigma_j}{1-\eta}+\frac{\pi}{4}\beta p\sigma_i^2+\beta V_{\rm int}(i)\ . \tag{9}$$

Consider the *excess* chemical potential $\mu_i^{\rm ex} = kT\ln\rho_i + W_i$. Putting Eqs. (8) and (9) into (6) gives

$$\beta\mu_i^{\rm ex} = \ln\rho_i - \ln(1-\eta) + \frac{\pi}{2}\frac{\sigma_i \sum_j \rho_j\sigma_j}{1-\eta} + \frac{\pi}{4}\beta p\sigma_i^2 - \ln u_i + \ln C \ . \quad (10)$$

At equilibrium we must have $\mu_i = \mu_j$ equal to a constant κ for a given value of $\rho = \sum \rho_i$. Using Eq. (5) for the pressure we then get

$$\kappa(\rho) = \ln(n_i/u_i) + \frac{\pi}{2}\frac{(\sum_j \rho_j\sigma_j)\sigma_i}{1-\eta} + \eta\left[\frac{1}{1-\eta} + \frac{\pi}{4}\frac{(\sum_j \rho_j\sigma_j)^2}{\rho(1-\eta)^2}\right] . \quad (11)$$

If we have a binary mixture, then equating Eq. (11) for species 1 and 2 and putting $\rho_i = n_i\rho$ gives

$$\ln\left[\frac{n_1}{n_2}\frac{u_2}{u_1}\right] + \frac{\pi}{2}\frac{\rho(\sigma_1-\sigma_2)\bar{\sigma}}{1-\eta} + \frac{\pi}{4}\frac{\rho(\sigma_1^2-\sigma_2^2)}{1-\eta} + (\sigma_1^2-\sigma_2^2)\left[\frac{\pi}{4}\frac{\rho\bar{\sigma}}{1-\eta}\right]^2 = 0 \ , \quad (12)$$

where $\bar{\sigma} = n_1\sigma_1 + n_2\sigma_2$. Consider

$$\xi = \frac{4}{\pi\rho} - (n_1\sigma_1^2 + n_2\sigma_2^2) = \frac{4}{\pi\rho}(1-\eta) \ . \quad (13)$$

Multiplying Eq. (12) through by ξ^2 ($\neq 0$) gives

$$\xi^2\ln\left[\frac{n_1}{n_2}\frac{u_2}{u_1}\right] + \xi(\sigma_1-\sigma_2)[(\sigma_1+\sigma_2)+2\bar{\sigma}] + (\sigma_1^2-\sigma_2^2)\bar{\sigma}^2 = 0 \ . \quad (14)$$

This is a quadratic in ξ and can be solved analytically for a given value of n_1: $0 < n_1 < 1$, $n_1 + n_2 = 1$. The negative solution to Eq. (14) is discarded as being unphysical. The equation of state can then be calculated as a parametric equation in n_1 from Eq. (5).

IV. SIMULATIONS

A. Constant *NpT* Monte Carlo simulations

The simulation techniques used for the binary mixtures are very similar to those described in I for single-species systems. Here we will only describe the modifications required for binary mixtures. The positional moves of the particles and the scaling moves of the system were made precisely as described in I. A scaling of the system was attempted once every Monte Carlo cycle (positional move per particle). Binary mixtures of disks required a further move consisting of a change in disk size. Consider a mixture of disks of sizes σ_1 and σ_2 ($\sigma_1 > \sigma_2$) and degeneracies D_1 and D_2 ($D_1 > D_2$), as defined in Eq. (7). For a given disk of size σ_i a trial disc size σ_j was chosen with probability $P(j)$ where

$$P(j) = u_j = \frac{D_j}{D_1 + D_2} \ . \quad (15)$$

Moves which would result in overlap were rejected. A change of disk size was attempted before each positional move.

B. The Voronoi tesselation

The Voronoi tesselation of the binary mixture was constructed as described in I with the centers of mass of the disks as seed points for the tesselation. The different disk sizes required a minor modification to the setting up of the initial configuration as described in I for single-species systems. For the binary mixtures, the seed points were randomly allocated to a species according to the degeneracies D_1 and D_2. The diameters of the hard disks were then assigned with $\sigma_2 < \sigma_1 = d_{\rm min}$, the minimum nearest-neighbor separation.

The Voronoi tesselation was dynamically maintained throughout the Monte Carlo simulations. The method used is described in I and does not depend on the number of species in the system. It was thus used unmodified.

In studying the Voronoi tesselations of single-species hard-disk systems, we found that the distribution of Voronoi edge lengths $p(d)$ can be fitted by the sum of two Gaussian functions, as described in I. The fits obtained are good at all densities, and the fitting parameters are found to reflect structural properties of the disk systems.

The distribution functions $p(d')$ obtained from the Monte Carlo simulations were fitted by a function of the form

$$g(d') = \frac{1}{\sqrt{\pi}\omega_1} I_1 \exp\left[-\frac{(d'-Q_1)^2}{\omega_1^2}\right] + \frac{1}{\sqrt{\pi}\omega_2} I_2 \exp\left[-\frac{(d'-Q_2)^2}{\omega_2^2}\right] , \quad (16)$$

where $d' = d/\sigma_2$. The parameters Q_1, Q_2, $W_1 = (\omega_1 \ln 2)$, and $W_2 = (\omega_2 \ln 2)$ represent the means and widths of the two Gaussians in units of σ_2. I_1 and I_2 give the areas under each of the two Gaussians. Values for the parameters were obtained by a least-squares fit to the Monte Carlo data. The term "main Gaussian" will refer to the Gaussian which is mainly responsible for the peak in the distribution function $p(d')$ and its fit parameters will be denoted by the subscript 1. The other Gaussian, the "secondary Gaussian", will be denoted by the subscript 2.

As in I, we emphasize that the functional form of $g(d')$ has no physical basis. The fit used is found to be a useful tool that provides an excellent way of looking at the structure of the systems.

V. RESULTS

The mixtures studied here are unusual in that the relative concentrations of the species are allowed to vary. The simulations are therefore not at fixed composition. As described in Sec. III, it is possible to use scaled-particle theory, and in particular Eqs. (5) and (11), to pre-

dict the packing-fraction concentration profile and the equation of state given $\chi=\sigma_1/\sigma_2$ and $\nu=D_1/D_2$. We will look first at systems for which "interesting" behavior is predicted to occur in the fluid phase, well away from the liquid-solid transition region. For convenience we will refer to the loci of data for the single-species systems (from I) as the *base curves* or *lines*. Below we describe our results for four different cases corresponding to different values of ν and χ.

A. $\nu=9, \chi=1.5$

Systems of 225 disks with $\nu=9$ and $\chi=1.5$ were first considered. Equilibration runs of 10 000 cycles were performed followed by production runs of 10 000 cycles. Snapshots taken at the end of the production runs are shown in Figs. 1(a)–1(d). The lowest-density system already has a significant proportion (45%) of small disks. As the density increases, the concentration of large disks decreases, as expected. The systems are sufficiently fluid at all densities considered that the smaller population is randomly distributed within the larger population. Figure 2 shows the packing-fraction concentration profile. The solid line gives the SPTD prediction and the points are from the Monte Carlo simulations. The agreement is excellent, even at very low concentrations.

Figure 3 gives the fit parameters Q_1 and Q_2 from the Voronoi edge-length distributions as a function of reduced pressure. The solid lines are the base curves from the single disk species results (from I). The mean of the secondary Gaussian is within the estimated errors of the base curve, except for the lowest-density data, which show some scatter and lie slightly above the curve. For the highest densties, for which the concentration of large disks is very small, the values of Q_1 fall upon the base curve. The deviation of the data from the base curve at lower densities increases with increasing large-disk concentration. Since the Voronoi edge-length distributions are normalized with respect to the smaller-disk diameter, the presence of larger disks in the systems causes an effective change of scale. The slight shift of the Q_2 data at the lowest densities is consistent with the shift in Q_1.

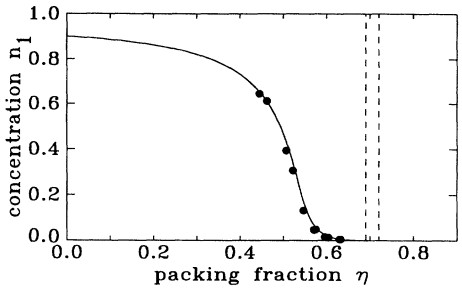

FIG. 2. The concentration of large disks n_1 as a function of packing fraction for mixtures of 225 hard disks with $\nu=9$ and $\chi=1.5$. The dashed lines give the liquid-solid transition region for the single species systems (from I).

B. $\nu=19, \chi=1.15$

To see how the packing-fraction concentration profile is affected by thermodynamic equilibrium, a system of 256 disks with $\nu=19$ and $\chi=1.15$ was studied purely from compression runs, with large applied pressure. This choice of ν and χ also places the middle of the large-small transition coincident with the start of the liquid-solid transition. The data points were each averaged over only 1000 cycles. For 1000 cycles, a change in disk size to a small disk would be attempted, on average, 50 times per disk, so although the systems would not be in thermo-

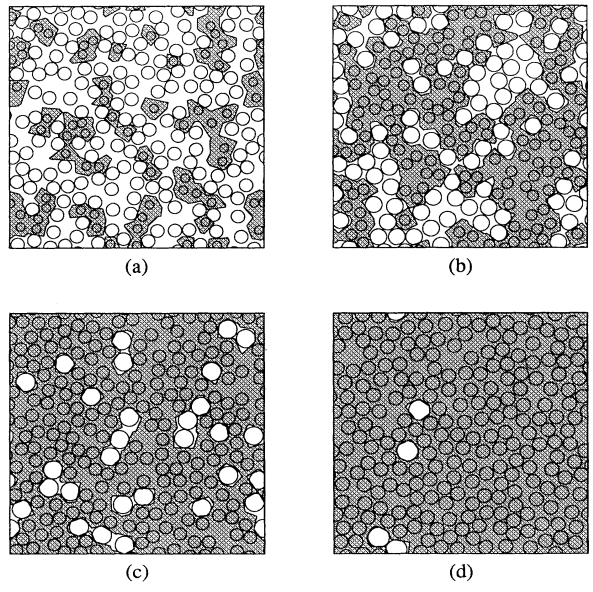

FIG. 1. Snapshots of configurations of mixtures of 225 hard disks, with $\nu=9$ and $\chi=1.5$, at pressures p/kT of (a) $1.72\sigma^{-2}$ (b) $2.57\sigma^{-2}$, (c) $3.46\sigma^{-2}$ (d) $4.37\sigma^{-2}$. The systems are scaled to the same box size and the shaded regions indicate the Voronoi polygons associated with the smaller disks.

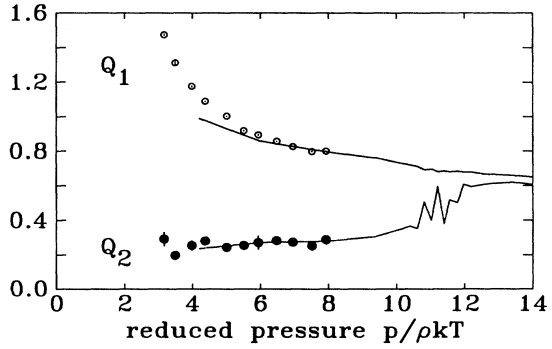

FIG. 3. The fit parameters Q_1 (○) and Q_2 (●) as functions of reduced pressure for mixtures of 225 hard disks with $\nu=9$ and $\chi=1.5$. The error bars for Q_1 are within the open circles. The solid lines are the base curves (from I).

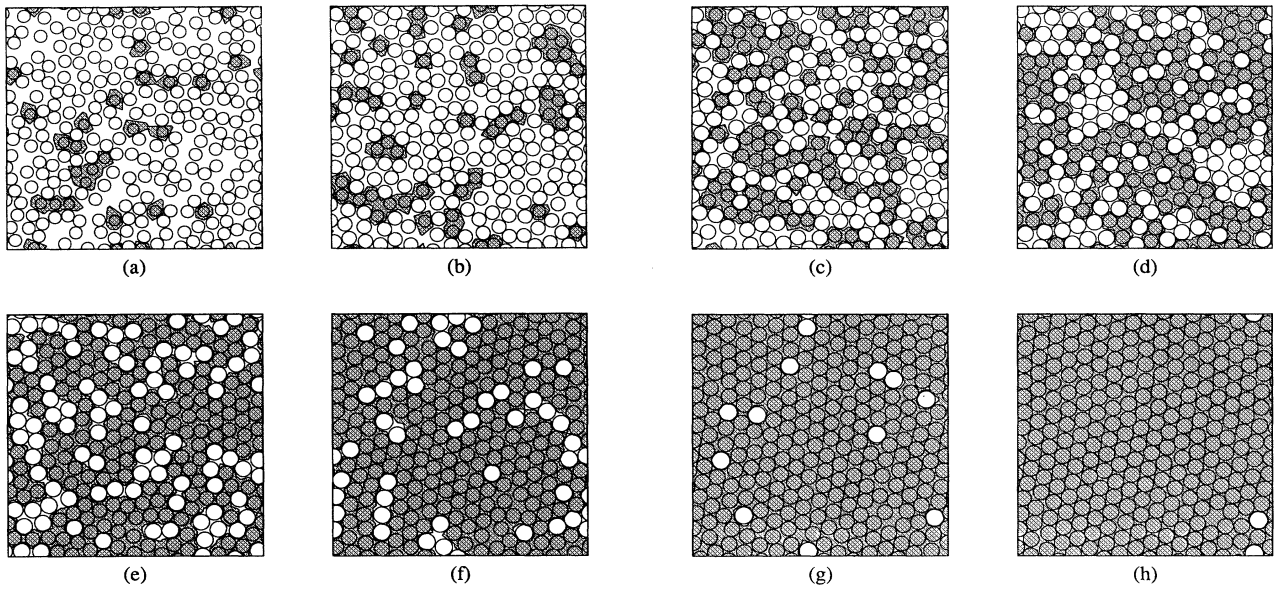

FIG. 4. Snapshots of configurations of mixtures of 256 hard disks, with $\nu=19$ and $\chi=1.15$, at intervals of 5000 Monte Carlo cycles. These nonequilibrium systems have high applied pressures p/kT of (a) $6.38\sigma^{-2}$ (b) $7.74\sigma^{-2}$, (c) $17.4\sigma^{-2}$ (d) $18.1\sigma^{-2}$, (e) $27.9\sigma^{-2}$, (f) $28.9\sigma^{-2}$, (g) $40.0\sigma^{-2}$, (h) $41.7\sigma^{-2}$. The systems are scaled to the same box size and the shaded regions indicate the Voronoi polygons associated with the smaller disks.

dynamic equilibrium they would be expected to be near equilibrium with respect to concentration. Snapshots of some of the configurations are shown in Figs. 4(a)–4(h). At low densities [Figs. 4(a) and 4(b)] the small disks that are present are scattered randomly through the system. The number of small disks increases with density. As the packing fraction approaches η_{liq}, the liquid edge of the transition region for single species disk systems [Fig. 4(c)], there are roughly equal numbers of large and small disks. Within the transition region [Fig. 4(d)], the large disks appear to want to form crystalline domains, where there are sufficient large disks to do so. The regions of small disks are still liquidlike, though there is some ordering next to the larger disks. As the number of small disks increases with density, η now at η_{sol}, the solid edge of the transition region [Fig. 4(e)], they start to order. Now, though, there are insufficient large disks for large-disk domains and they tend to be disordered between the regions of more-ordered small disks. At the higher densities [Figs. 4(f)–4(h)] there are relatively few large disks. Their presence is, however, enough to disrupt the packing of the smaller disks. Only at the highest densities is the small-disk phase able to form a single ordered region.

The packing-fraction concentration profile is shown in Fig. 5 on a semilog plot. The dashed lines give the position of the single species transition region, and the inset illustrates the superposition of the two transitions. The solid curve is the SPTD prediction. The agreement of the data with the SPTD prediction is remarkable. Not only are the 1000 cycles sufficient to give concentration equilibrium at a given average density, but scaled-particle theory is seen to predict the packing-fraction concentration profile accurately, for these systems, in both the fluid *and solid* phases.

C. $\nu=99, \chi=1.15$

Larger systems of 440 disks with $\nu=99$ and $\chi=1.15$ were studied, with equilibration runs of 5000 cycles and

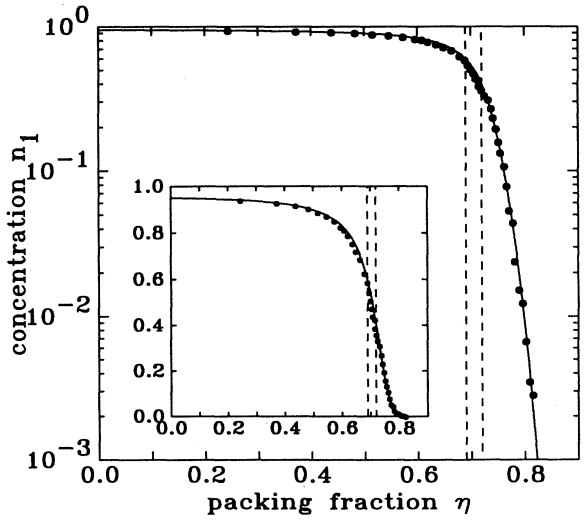

FIG. 5. The concentration of large disks n_1 as a function of packing fraction for mixtures of 256 hard disks with $\nu=19$ and $\chi=1.15$. The dashed lines give the liquid-solid transition region for the single species systems (from I).

production runs of 10 000 cycles. Snapshots of some of the systems are shown in Figs. 6(a)–6(h). There are still relatively few small disks in the systems right up to the start of the liquid-solid transition, and all the systems are disordered. Within the liquid-solid transition region [Figs. 6(d) and 6(e)], the large disks form more-ordered domains. The small disks are found between these domains and within less-ordered, fluidlike regions. At packing fractions slightly higher than η_{sol} [Fig. 6(f)], the ordered domains are much larger, and many of the small disks take on the same order as the large disks. There are still a few disordered regions within the systems. The number of small disks starts to increase noticeably once the structure becomes almost fully ordered. At the highest densities, there are few large disks in the systems.

The packing-fraction concentration profile is shown in Fig. 7. The solid line is the SPTD data and the dashed lines give the liquid-solid transition region. The inset shows the same data on a semilog plot. At low densities, up to the liquid-solid transition region, and at very high densities, there is very good agreement between the Monte Carlo data and the SPTD data. Within the transition region, the number of large disks actually *increases* slightly. At densities with η just above η_{sol} the curve appears to follow a path parallel to the SPTD curve, but displaced to higher packing fractions. Then, as the density is increased, the concentration drops rapidly until it rejoins the SPTD curve at higher densities. The start of this drop corresponds to the density at which the systems are fully ordered, though they do contain defects. The sharpness of the drop is most apparent on the semilog plot. The deviation of the Monte Carlo data from the SPTD data is simply a result of packing considerations. In response to the applied pressure, the system wants to reduce its area. it can do this either by reducing its "free area," which requires an increase in its order at these densities, or by reducing the total area of the disks and leaving the free area the same. Across the liquid-solid transition region, the increase in order within the large disks is sufficient to also allow an increase in the number of large disks. The number then reduces gradually, while the amount of order in the system increases further. Once the system becomes fully ordered, however, the only way to reduce the area is to reduce the number of large disks. Scaled-particle theory predicts a drop in large-disk concentration at a lower density, since it does not take ordering effects into consideration.

Figure 8 shows the fit parameters Q_1 and Q_2. The solid lines show the base curves (from I). The data for Q_1 lie consistently higher than the base curve for the low-density systems. At a point which corresponds to the start of the large-small transition, Q_1 starts to drop towards the base curve. At higher densities, the data would appear to follow the base curve. Exactly the same analysis applies to the data for Q_2. The fractional increase in the values of Q_1 and Q_2 at the lower densities corresponds to $\chi=1.15$, that is, the ratio of the disk sizes. If the edge lengths were normalized by σ_1 rather than σ_2 at these densities, then the data for Q_1 and Q_2 would fall on the base curves. The shift is therefore due to a scaling of the typical length in the system. The effect of the liquid-solid transition on Q_2 is the same as for the single species disk systems. The large-small transition has no affect on Q_2 other than the scaling described above, which is consistent with the observed scaling of Q_1.

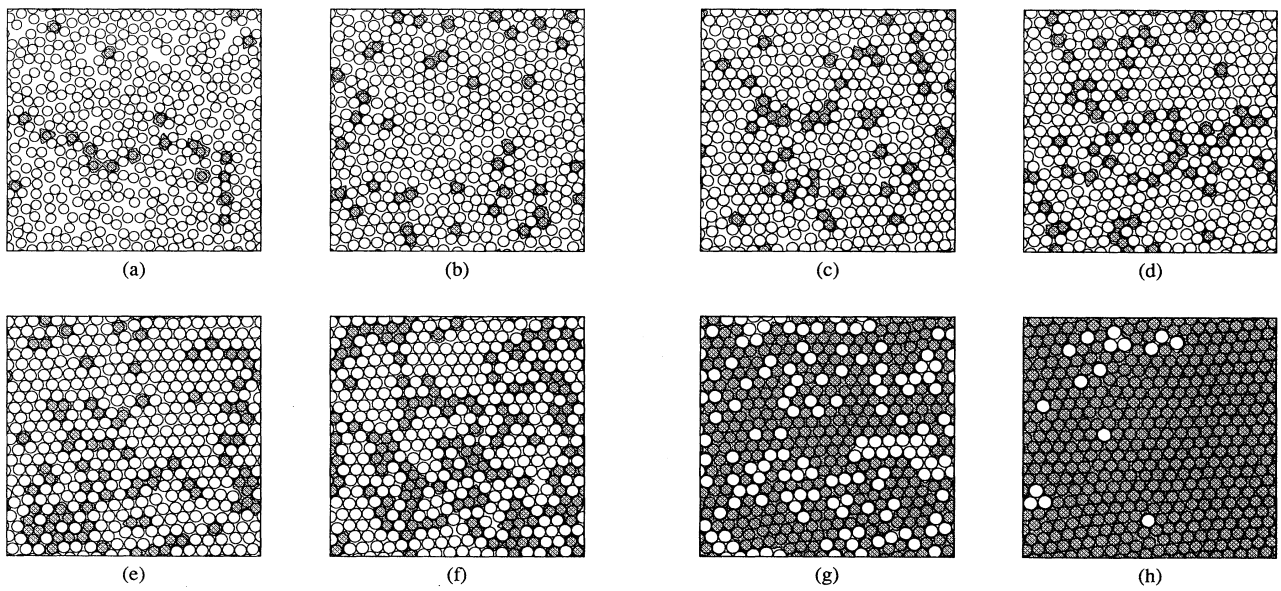

FIG. 6. Snapshots of configurations of mixtures of 440 hard disks, with $\nu=99$ and $\chi=1.15$, at pressures p/kT of (a) $2.79\sigma^{-2}$, (b) $5.86\sigma^{-2}$, (c) $7.14\sigma^{-2}$, (d) $8.51\sigma^{-2}$, (e) $10.5\sigma^{-2}$, (f) $12.0\sigma^{-2}$, (g) $13.9\sigma^{-2}$, (h) $16.4\sigma^{-2}$. The systems are scaled to the same box size and the shaded regions indicate the Voronoi polygons associated with the smaller disks.

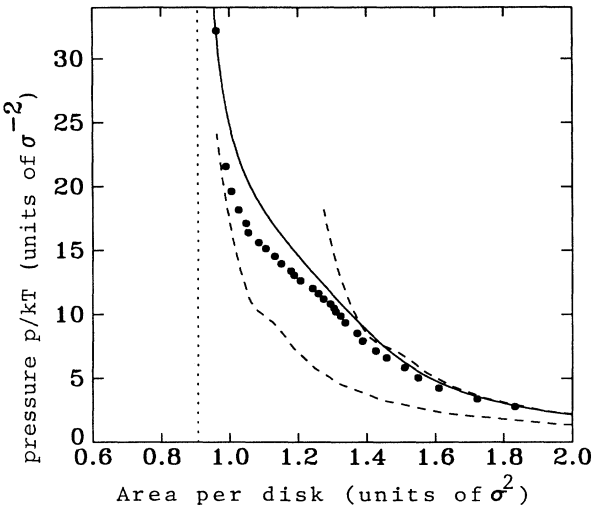

FIG. 7. The concentration of large disks n_1 as a function of packing fraction for mixtures of 440 hard disks with $\nu=99$ and $\chi=1.15$. The dashed lines give the liquid-solid transition region for the single species systems (from I).

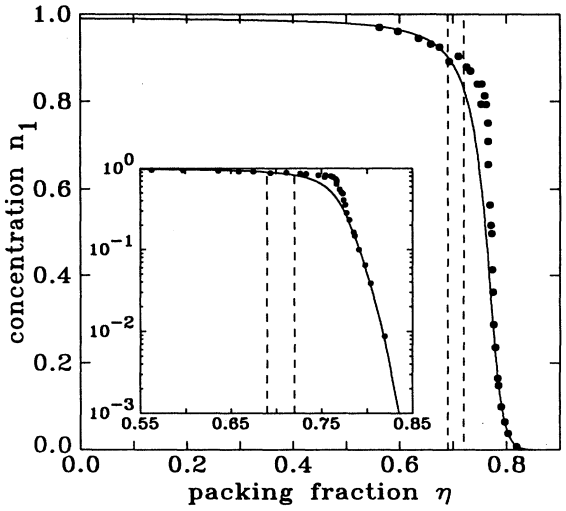

FIG. 9. Lateral pressue as a function of area per disk for mixtures of 440 disks with $\nu=99$ and $\chi=1.15$. The points (●) are Monte Carlo data, the solid line is data from the SPTD Eqs. (5) and (14). The dashed lines are the true and scaled base curves (from I) as described in the text. The dotted line is the high-density limit $A=\pi\sigma_2^2/2\sqrt{3}$.

The p-A isotherm for this system is shown in Fig. 9. The lower dashed line in the figure is the base curve from Fig. 13 of I. The upper dashed curve is the same curve but is scaled in both axes, so that it corresponds to a system with disk diameters of 1.15σ. The Monte Carlo data can be divided into three regions. At low densities, the data follow the scaled base curve, but at a slightly reduced pressure. At high densities, the data join then follow a projection of the base curve. In the intermediate region, the data follow an almost straight path from the scaled base curve to the true base curve. This is the transition region for a transition from a predominantly large-disk system to a predominantly small-disk system. The low-density limit of the large-small transition region, as apparent from the p-A isotherm, corresponds to the density at which the system first becomes fully ordered. The high-density limit corresponds to the point at which the Monte Carlo data rejoin the SPTD data on the density-concentration plot. It should be noted that there is no evidence in this plot to suggest the presence of a liquid-solid, order-disorder transition.

The SPTD data, shown as a solid line, lie slightly above the Monte Carlo data at low densities. The data are also seen to cross to the base curve, but at a higher pressure than that of the simulation data for the base curve. The data point of the highest-density binary system is seen to lie on the SPTD curve. This does not imply that the SPTD data are good at high densities; rather, that the two data curves only cross at this point. The dotted line is the area corresponding to a close-packed system, $A=\pi\sigma^2/2\sqrt{3}$, which is the correct asymptote for hard-disk, p-A data. In contrast, the SPTD data have an asymptote at $A=0$.

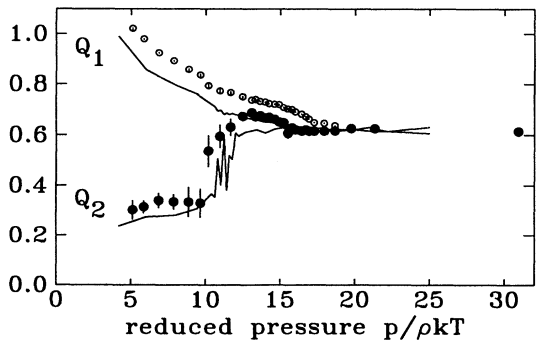

FIG. 8. The fit parameters Q_1 (○) and Q_2 (●) as a function of reduced pressure for mixtures of 440 hard disks with $\nu=99$ and $\chi=1.15$. The error bars for Q_1 are within the open circles. The solid lines are the base curves (from I).

D. $\nu=10^5, \chi=2$

Systems of 440 disks with $\nu=10^5$ and $\chi=2$ were studied following the methods employed with the previous binary systems. Unless prohibitively long equilibration runs are made, the systems are prevented from attaining true equilibrium by the high value of ν combined with the relatively large difference in disk sizes. Fast compression and expansion runs were therefore performed in addition to slower compression and expansion runs, closer to equilibrium. For the fast compression run a very high pressure of $p/kT=300\sigma^{-2}$ was applied and statistics were averaged every 5000 cycles over a total of 7×10^5 cycles. A low pressure of $1.0\sigma^{-2}$ was then applied and the system was allowed to expand over a total of 35 000 cycles. Statistics were averaged every 1000 cycles. For the

slower compression run, the pressure was incremented $0.2\sigma^{-2}$ every 15 000 cycles up to a pressure of $15.0\sigma^{-2}$. The slow expansion run was similarly performed with the applied pressure being reduced by $0.2\sigma^{-2}$ every 15 000 cycles. This expansion was then repeated from an applied pressure of $4.4\sigma^{-2}$ with the same pressure decrement every 30 000 cycles.

Figures 10(a)–10(h) show snapshots of systems from the slower compression run with pressures from 2.0 to $15.0\sigma^{-2}$. The concentration of small disks remains very low through the liquid-solid transition [Figs. 10(a) and 10(b)]. At these pressures the system behaves as if it contained only large disks. As the pressure increases, the number of small disks increases. Most of the large disks are in solidlike, ordered domains, and the small disks tend to form disordered regions between these domains [Figs. 10(c) and 10(d)]. As the small-disk concentration increases further, the large-disk domains become much smaller, and many of the large disks are in small, isolated groups. Some of the small disks then start to order, though the structure of the system is still predominantly disordered [Fig. 10(f)]. Increasing the pressure further takes the system from this small-disk fluid through another liquid-solid transition to a small-disk solid [Fig. 10(h)].

Snapshots are shown in Figs. 11(a)–11(h) for the slower expansion run. The expansion of the system essentially sees a reversal of the phase behavior observed during the compression run. The slightly lower applied pressure first allows the final configuration of the compression run to equilibrate further. The few remaining large disks in the system disappear and the small-disk solid becomes almost fully ordered [Fig. 11(a)]. As with the single-sized disk systems studied in I, this system cannot be truly commensurate with the simulation cell. The ordered structure melts to a small-disk fluid as the pressure is reduced [Fig. 11(b)]. Large disks appear within the system as the pressure is reduced, and where they form large enough groups, they start to order [Fig. 11(e)]. As the large-disk concentration increases further with decreasing pressure, the larger large-disk domains do not order fully [Figs. 11(f) and 11(g)]. The regions containing the last of the small disks remain disordered, and then the large-disk domains themselves start to melt, and a large-disk fluid is finally obtained [Fig. 11(h)].

An even slower expansion from a pressure of $4.4\sigma^{-2}$ produced configurations which differed little from those shown in Fig. 11, except that the structures observed were shifted slightly in pressure.

The configurations from the fast compression and expansion runs were also similar to those of the slower runs. There were several noticeable differences, however. As the large-disk concentration decreased, the remaining large disks appeared to be quite randomly distributed throughout the system. This is in contrast to the ordered domains apparent in the systems shown in Fig. 10. The final small-disk solid consisted of several large domains of ordered disks. For these to merge into a single, large ordered domain would require a significant rearrangement of most of the structure. The system has thus quenched into a structure reminiscent of a glass or a polycrystalline aggregate. During the rapid expansion, the structure remained disordered. The large disks again appeared to be randomly distributed throughout the system, and there was no indication that they would prefer to form more-ordered domains.

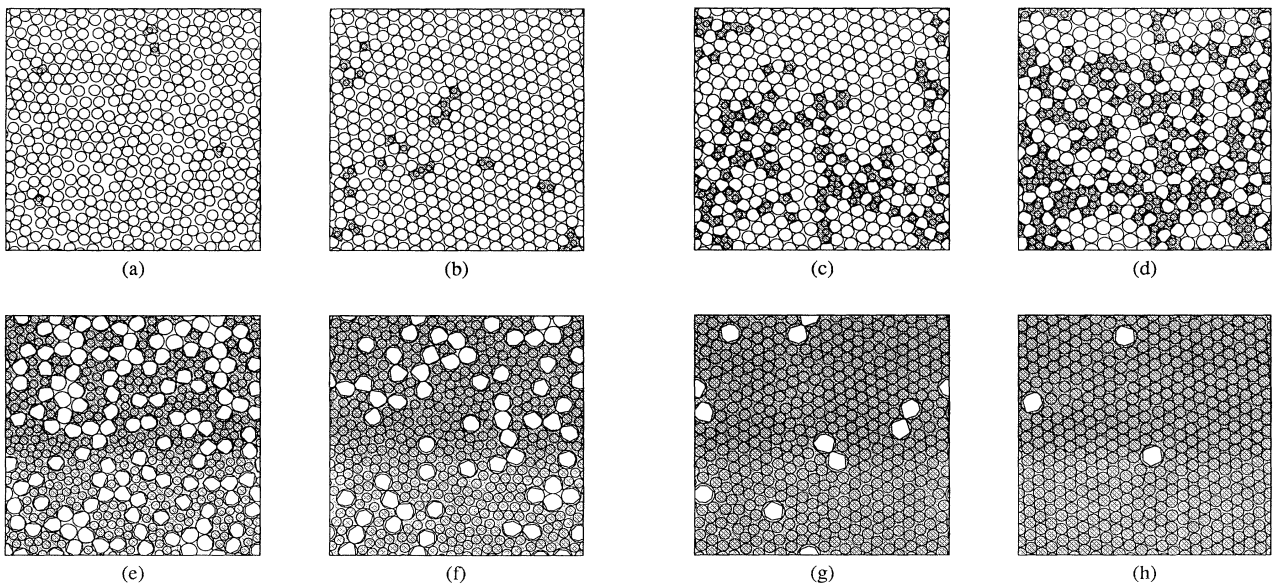

FIG. 10. Snapshots of configurations of mixtures of 440 hard disks, with $\nu=10^5$ and $\chi=2$, for the slow compression run at pressures p/kT of (a) $2.0\sigma^{-2}$, (b) $3.0\sigma^{-2}$, (c) $5.4\sigma^{-2}$, (d) $6.0\sigma^{-2}$, (e) $8.2\sigma^{-2}$, (f) $10.0\sigma^{-2}$, (g) $12.0\sigma^{-2}$, (h) $15.0\sigma^{-2}$. The systems are scaled to the same box size and the shaded regions indicate the Voronoi polygons associated with the smaller disks.

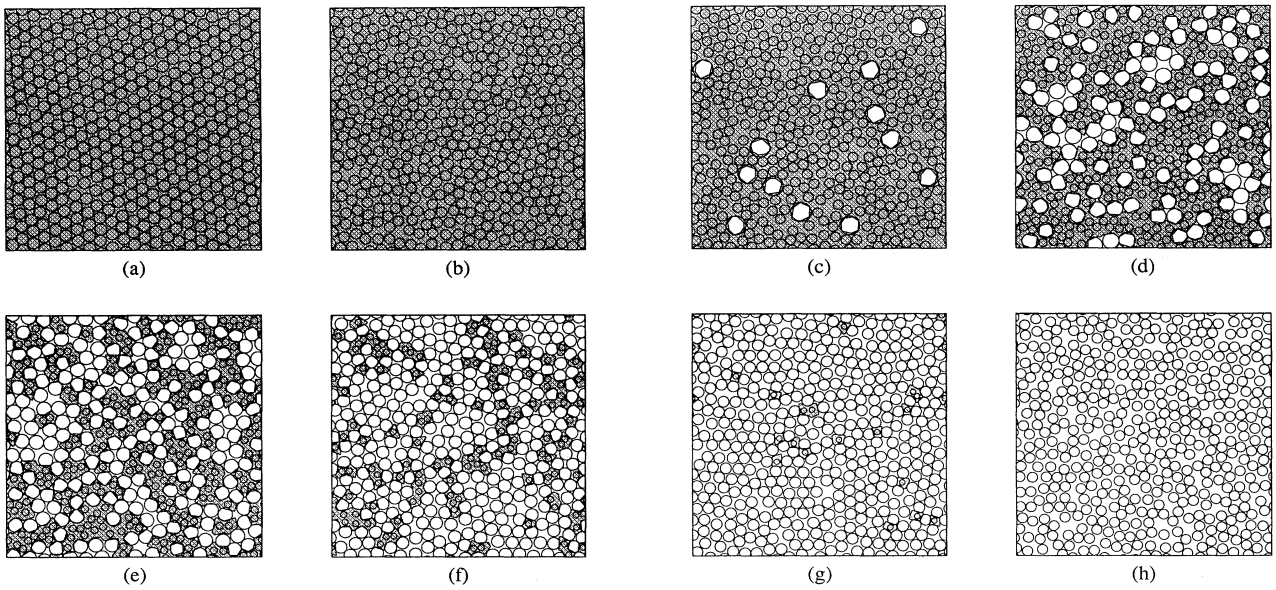

FIG. 11. Snapshots of configurations of mixtures of 440 hard disks, with $\nu=10^5$ and $\chi=2$, for the slow expansion run at pressures p/kT of (a) $12.0\sigma^{-2}$, (b) $6.0\sigma^{-2}$, (c) $4.0\sigma^{-2}$, (d) $3.0\sigma^{-2}$, (e) $2.6\sigma^{-2}$, (f) $2.2\sigma^{-2}$, (g) $1.8\sigma^{-2}$, (h) $1.0\sigma^{-2}$. The systems are scaled to the same box size and the shaded regions indicate the Voronoi polygons associated with the smaller disks.

The large-disk concentration n_1 is shown as a function of area per disk in Fig. 12(a). The solid points correspond to the two compression runs, and the open points correspond to the expansion runs. The central solid line gives the SPTD prediction for this system. The two outer curves are derived from the SPTD data by shifting the area by $\pm\delta A$. Here, δA is given by half the difference between the fast compression and fast expansion results at $n_1=0.5$. The shoulders in the compression data at $n_1\sim 0.95$ are probably due to initial packing conditions in the solid, as found in the $\nu=99$ systems. The Monte Carlo data would appear to follow lines roughly parallel to the SPTD prediction for concentrations of between 0.05 and 0.8. This is quite remarkable, since the structures of the systems in all the runs changed considerably over this range. It can also be seen that, for the expansion runs, doubling the number of Monte Carlo cycles between successive decrements in the pressure from 15 000 to 30 000 has little effect on the large-disk concentration as a function of area. There is also little change when the concentration is plotted as a function of packing fraction, as shown in Fig. 12(b). The shoulders in the compression data are much more apparent than in Fig. 12(a). The dashed lines, which indicate the packing fractions at the liquid and solid edges of the transition region in single species disk systems, no longer serve to indicate the ordered or disordered nature of the systems at intermediate concentrations. Where the slow compression data come close to $\eta_{\rm sol}$, for $n_1\lesssim 0.3$, the systems are disordered, and where the slow expansion data come close to $\eta_{\rm liq}$, for $n_1\gtrsim 0.7$, the systems contain a number of regions of ordered large disks.

Figure 13 shows the fit parameters Q_1 and Q_2 as functions of pressure for the slow compression and expansion runs. Note that Q_1 and Q_2 no longer scale simply with the base curves, as they would do if plotted as a function of reduced pressure. As with all other systems studied, Q_1, for the slow compression run, varies smoothly with pressure. Q_2, however, varies quite dramatically across the range of pressures studied here. At the lowest pressures, Q_2 is about twice that of the base curve in the fluid phase. This scaling is due to the disk-size ratio $\chi=2$. Between pressures of about $2.6\sigma^{-2}$ and $3\sigma^{-2}$ there is a marked jump corresponding to the large-disk liquid-solid transition. Q_2 remains at around the same value until the pressure reaches $4.2\sigma^{-2}$. At this point the concentration of small disks starts to increase, and the regions in which they appear become disordered. Q_2 drops almost linearly with increasing pressure until a pressure of around $5.2\sigma^{-2}$, at which point about a third of the system is disordered. Q_2 continues to drop, though not as quickly, as more small disks appear in the system and the regions of ordered large disks break up. At a pressure of around $8\sigma^{-2}$, the remaining groups of large disks are quite small, and as they dissappear Q_2 drops more quickly again with increasing pressure until a pressure of $9.4\sigma^{-2}$ is reached. There are now few large disks in the system and the structure is totally disordered. Q_2 remains constant until a pressure of around $12\sigma^{-2}$, whereupon it starts to rise again. At a pressure of $13\sigma^{-2}$ there is a jump in Q_2 and it joins Q_1 on the base curve. This corresponds to the small-disk liquid-solid transition.

For the slow expansion run, Q_1 follows the base curve

right down to a pressure of about $4\sigma^{-2}$. There are still very few large disks in the system at this point. Q_1 then starts to increase as the large-disk concentration increases. Q_2 follows the base curve down to a pressure of $12.8\sigma^{-2}$. There is then a slight drop in Q_2 as the pressure drops to $12.4\sigma^{-2}$. During this period the few large disks that remain in the system dissappear. This drop in Q_2 is the same as that observed in I for a crystalline system incommensurate with the simulation box. Here the system is seen to form one large crystalline domain [Fig. 11(a)]. As the pressure is further reduced, Q_2 drops slowly until a pressure of $8.6\sigma^{-2}$. It then drops suddenly down to the base curve as the system melts and passes through a small-disk solid-liquid transition. As the first large disks start appearing in the system at a pressure of around $5\sigma^{-2}$, Q_2 drops more quickly. However, once there are enough large disks to start forming ordered groups, Q_2 rises quite rapidly until most of the disks are large, whereupon it starts to drop again. This maximum corresponds to the pressures at which there is most order within the groups of large disks. At the higher pressures there are many disordered regions containing both large and small disks. At the lower pressures there are few small disks, but the regions of large disks have started melting. The results for the slower expansion run (for pressures below $4.4\sigma^{-2}$) differ from those of the slow expansion run only in that the maximum described above occurs at a slightly higher pressure ($2.4\sigma^{-2}$ instead of $2.0\sigma^{-2}$) and has a slightly higher value of Q_2.

To eliminate the effects of disk size on the behavior of Q_2 we define $\psi = Q_2/Q_1$. Figure 14 shows that ψ behaves much like an order parameter, though we emphasize that there is nothing to prevent it from increasing above unity. Also shown in Fig. 14 is the defect density $N_{\rm def}$, defined as in Eq. (5) of I to be the fraction of particles with other than six nearest neighbors. The behavior of ψ is, predictably, very similar to that of Q_2. For the slow compression run [Fig. 14(a)], $N_{\rm def}$ appears to tell us little about the changing structure of the system. Apart from a slight kink at a pressure of $12.6\sigma^{-2}$, which is close to the small-disk liquid-solid transition, all other changes in the slope of $N_{\rm def}$ are at different pressures to those of ψ. This is not the case, however, for the slow expansion run [Fig. 14(b)]. For all pressures right down to $4\sigma^{-2}$, $N_{\rm def}$ mimics the behavior of ψ. The drop in ψ at a pressure of $12.6\sigma^{-2}$ is reflected by a drop in $N_{\rm def}$ down to zero. This is con-

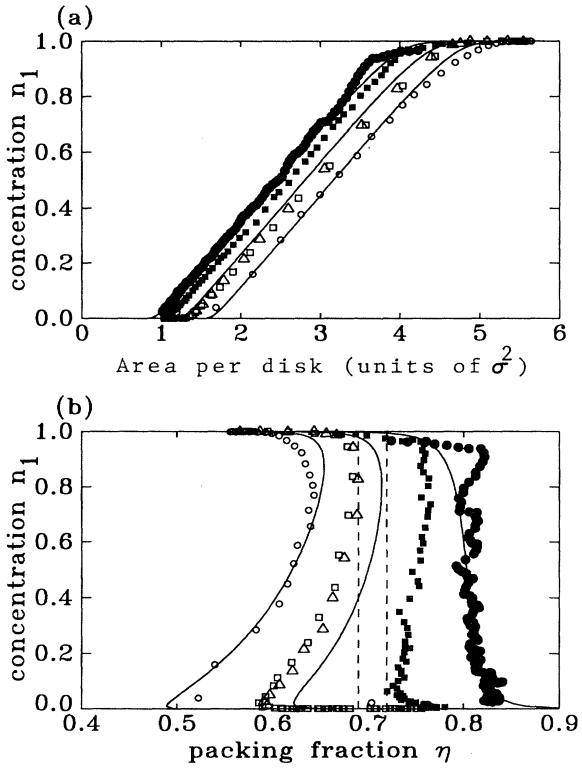

FIG. 12. The concentration of large disks n_1 as a function of (a) area per disk and (b) packing fraction for mixtures of 440 hard disks with $\nu = 10^5$ and $\chi = 2$, for the fast compression (●) and expansion (○) runs, the slow compression (■) and expansion (□) runs, and the slower expansion run (△). The solid lines give the normal and shifted SPTD data, as described in the text, and the dashed lines in (b) give the liquid-solid transition region for the single species systems.

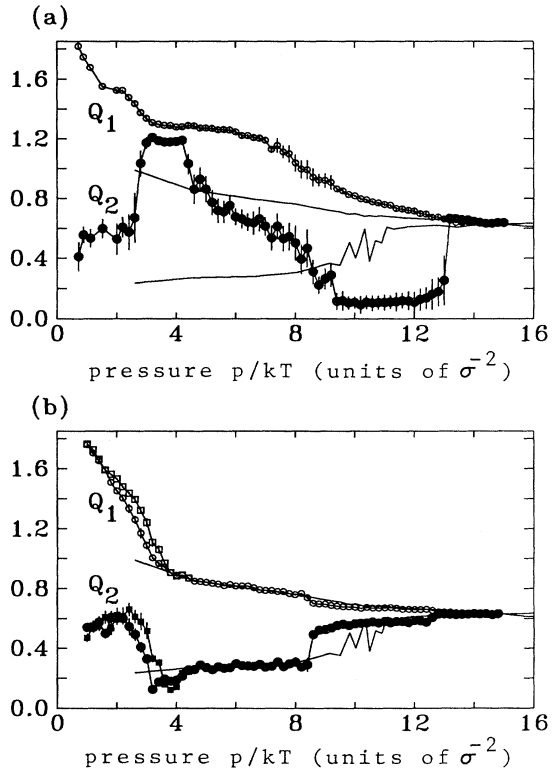

FIG. 13. The fit parameters Q_1 (○) and Q_2 (●) as functions of pressure for mixtures of 440 hard disks with $\nu = 10^5$ and $\chi = 2$. The data for the slow compression run are shown in (a) and data for the slow expansion run in (b). Also shown in (b) are the data for the slower expansion run (□,■). The solid lines are the base curves (from I).

sistent with the evidence of the snapshots that the structure forms a single crystalline domain. The drop in ψ across the solid-liquid transition is accompanied by an increase in $N_{\rm def}$. $N_{\rm def}$ then continues to rise as ψ drops. There is a maximum in $N_{\rm def}$ as ψ rises sharply and then a minimum at a pressure slightly lower than that of the maximum in ψ. For the slower expansion run, the behavior of both ψ and $N_{\rm def}$ is shifted to slightly higher pressures.

It is noticeable that for the expansion runs, for pressures for which the area of the system varies slowly, the changes in $N_{\rm def}$ are in step with the changes in ψ (Q_2). These systems are likely to be close to equilibrium. for the lower pressures of the expansion runs, where the area changes rapidly, and for the compression run for which the rate of change of the area is significant, the changes in $N_{\rm def}$ appear to be out of step with the changes observed in ψ (Q_2). These systems are probably further from equilibrium than the high-pressure expansion ones. It can be surmised, therefore, that the extent to which changes in ψ and $N_{\rm def}$ are in step reflects how close to true equilibrium the systems are.

Figure 15 compares ψ for the slow compression run ψ_c and the slow expansion run ψ_e. It is noticeable that between pressures of $2.0\sigma^{-2}$ and $13\sigma^{-2}$ ψ_c and ψ_e are almost totally complementary. This is a quite remarkable hysteresislike behavior.

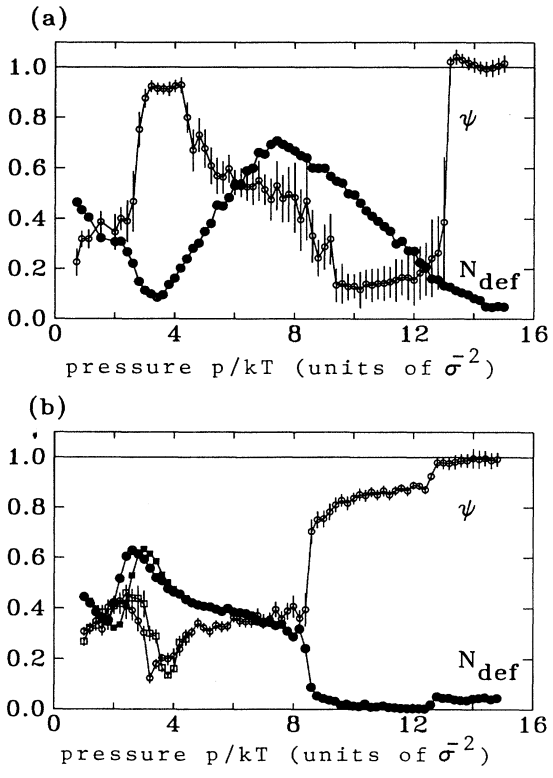

FIG. 14. The parameter ψ (○) and the number of defects $N_{\rm def}$ (●) for the slow compression run (a) and the slow expansion run (b) as functions of pressure for mixtures of 440 hard disks with $\nu=10^5$ and $\chi=2$. Also shown in (b) are the data for the slower expansion run (□,■).

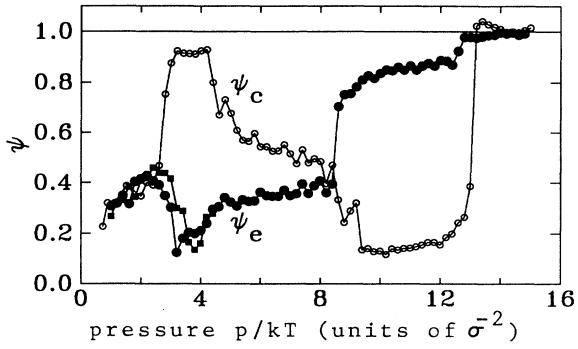

FIG. 15. A comparison of the parameter ψ for the slow compression run (○) and the slow expansion run (●) as a function of pressure for mixtures of 440 hard disks with $\nu=10^5$ and $\chi=2$. Also shown (■) are the data for the slower expansion run.

Although the fast nonequilibrium runs would appear to preclude looking at thermodynamic properties of the systems, we can make use of the SPTM of Eq. (5). The agreement of the SPT pressure (for general convex particles) with that from constant NpT Monte Carlo simulations has been shown in a previous paper[19] to be good for very dense systems of polydisperse hard-core triatomics. These systems did not exhibit an order-disorder transition. If a system is disordered, therefore, the SPTM of Eq. (5) should adequately predict the pressure of an equilibrium system with a similar structure, given the concentration n_1 and the area per disk. If there is significant order within the system, then the SPTM prediction for the pressure is likely to be high.

Keeping in mind that the SPTM pressure prediction will be high for systems with significant order, we now examine the p-A isotherms for both the compression and the expansion runs. These are shown in Fig. 16. The central solid line is data from the SPTD Eqs. (5) and (14). The other two solid lines are derived from the SPTD data by shifting the area by $\pm\delta A$ for a given large-disk concentration and recalculating the pressure from Eq. (5). The good agreement with the "fast" Monte Carlo data is consistent with Fig. 12(a). The data for the slow compression run are closer to, but still considerably higher than, the SPTD prediction. Slight kinks are apparent in the isotherm. These occur at pressures for which there are kinks or discontinuities in ψ (Q_2). For the slow expansion run, at pressures above $4.4\sigma^{-2}$, the area changes very little. A very slight shift in area can be seen between the data points for pressures of $8.4\sigma^{-2}$ and $8.6\sigma^{-2}$. This is the small-disk solid-liquid transition for which ψ changed dramatically from 0.7 to 0.4. As the pressure is reduced below about $4.4\sigma^{-2}$, the area starts to increase quite rapidly. At first, it would appear to be following a line between the SPTD curve and the fast expansion data. However, the data points gradually drop down to the fast expansion data. The area cannot expand as fast as it would like as a consequence of the dynamics

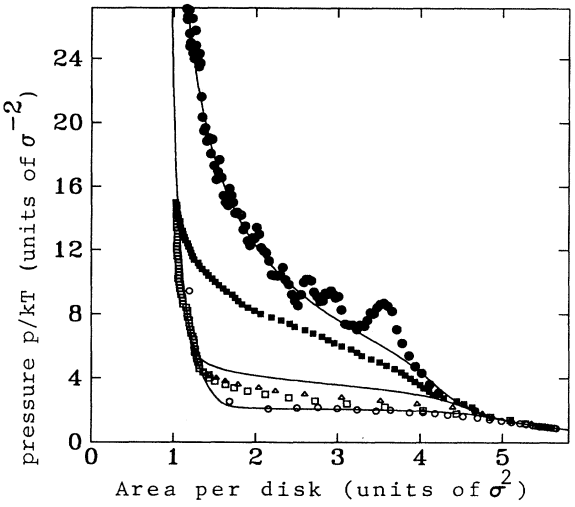

FIG. 16. Lateral pressure as a function of area per disk for mixtures of 440 disks with $\nu=10^5$ and $\chi=2$ for the fast compression (●) and expansion (○) runs, the slow compression (■) and expansion (□) runs, and the slower expansion run (△). The solid lines give the normal and shifted SPTD data as described in the text.

of the Monte Carlo simulation method. The maximum change allowed in the box length when the system is scaled (as described fully in I) is adjusted to keep a rejection ratio of 50%. When a very low pressure is applied to the system, nearly all trials which would result in a smaller system area are rejected and nearly all expansions are accepted. If the system is close to equilibrium, however, many more trials will be accepted for which the system area is reduced, and fewer will be accepted for which the area increases. The average area by which the system can increase per Monte Carlo cycle therefore greatly reduced. The slower expansion run data reflects this. Given twice as many cycles for each decrement in the pressure, the system can expand to a greater area. The isotherm is, therefore, flatter, and only rejoins the fast expansion data where this rejoins the SPTD curve.

In the next section we discuss how the results of this section can be used to describe the properties of lipid monolayers, with special reference to Fig. 16.

VI. SUMMARY AND CONCLUSIONS

In this paper we present a method for studying model mixtures of hard disks characterized by different disk sizes and preset internal degeneracies. The model incorporates both translational and internal degrees of freedom and may display cooperative phenomena in terms of these variables. The mixtures are studied by Monte Carlo simulation techniques, which faithfully account for the full statistical-mechanical problem, including the structural ordering transitions. We have also extended the scaled-particle theory for mixtures, which accounts for aspects of the packing properties of liquid phases but which neglects effects due to global ordering processes.

The simulations as well as the extended scaled-particle theory were applied to binary mixtures of disks of size ratio χ and degeneracy ratio ν. By varying χ and ν, the following possible scenarios were found as a function of increasing pressure [here we refer to a large-disk fluid (LF), a small-disk fluid (SF), a large-disk solid (LS) and a small-disk solid (SS)].

(a) ($\nu=9$, $\chi=1.5$.) A large-disk to small-disk transition followed by a liquid-solid transition:

$$\mathrm{LF}\rightarrow\mathrm{SF}\rightarrow\mathrm{SS}\ .$$

(b) ($\nu=99$, $\chi=1.15$.) A liquid-solid transition followed by a large-disk to small-disk transition:

$$\mathrm{LF}\rightarrow\mathrm{LS}\rightarrow\mathrm{SS}\ .$$

(c) ($\nu=19$, $\chi=1.15$.) A liquid-solid transition within a large-disk to small-disk transition:

$$\mathrm{LF}\rightarrow\mathrm{LF}+\mathrm{SF}\rightarrow\mathrm{LS}+\mathrm{SS}\rightarrow\mathrm{SS}\ .$$

(d) ($\nu=10^5$, $\chi=2$.) A liquid-solid transition and a large-disk to small-disk transition: compression,

$$\mathrm{LF}\rightarrow\mathrm{LS}\rightarrow\mathrm{LS}(+\mathrm{SF})\rightarrow\mathrm{LS}+\mathrm{SF}\rightarrow\mathrm{SF}(+\mathrm{LS})\rightarrow\mathrm{SS}\ ;$$

expansion,

$$\mathrm{SS}\rightarrow\mathrm{SF}\rightarrow\mathrm{SF}(+\mathrm{LF})\rightarrow\mathrm{LS}(+\mathrm{SF})\rightarrow\mathrm{LF}\ .$$

A surprising result is that the scaled-particle theory not only predicts the composition in the liquid phase, but also deep into the solid phase. However, in the transition region, where packing considerations cannot be neglected, the scaled-particle theory breaks down.

The main result of our model study is that there is an intricate interplay between packing and long-range positional ordering in mixed systems of disks of different sizes that may undergo size changes. This leads to unexpected results in the transition region with, for example, long-lived metastable granular configurations or reentrant ordering transitions, reminiscent of the reentrant phase behavior of Kr on graphite.[40]

The class of models for mixtures of hard disks introduced and studied in this paper has a general sphere of applicability. So far we have only explored the properties of the models in the case of a binary mixture, but extensions to multicomponent mixtures are straightforward. The special property of these models is that their composition is not an independent variable, but is instead determined by a set of intrinsic chemical potentials, whose values are fixed by the internal entropies associated with the disk degeneracies. These degeneracies can be interpreted as reflecting the statistics of internal state variables, for example, conformational states of a flexible molecule. Therefore, in their capacity of describing a system having positional as well as internal variables, the models become candidates for minimal models of lipid monolayers and bilayers.

The hard-disk models studied in the present paper, therefore, open up a novel and promising way of modeling the phase behavior of lipid monolayers spread on air-water interfaces.[41] Here we outline the perspectives of

such an approach by proposing the binary mixture model with $\chi \simeq 1-2$ and $\nu \gg 1$ as a minimal model of a lipid monolayer. In this model, the large-disk size corresponds to the extended (melted, conformationally disordered) acyl-chain state, and the small-disk size corresponds to the all-*trans* (confirmationally ordered) acyl-chain state. The large value of ν reflects the fact that the melted state carries a large internal entropy due to the many excitations of the disordered chain. The model is minimal in the sense that it only explores the effects of excluded volume and internal degrees of freedom and neglects direct, soft interactions.

Comparison of the model isotherms (Figs. 9 and 16) with experimental isotherms for monolayers of fatty acids and lipids (see, for example, Refs. 41–47 and references therein) suggests that the minimal model has captured the essential physics of these systems and hence underscores an earlier assertion by Nagle[48] that the excluded volume interactions are the dominant factor for their phase behavior. The nonzero slope of the isotherm at the start of the "plateau" region is quite reproducible for many experimental systems. Although the rate of compression of the monolayer has been observed to affect the isotherms across this plateau and at higher pressures,[49] even the use of very slow compressional speeds does not eliminate this positive slope. Furthermore, it is well accepted[50] that compressional-decompressional hysteresis is observed even at the slowest compressional speeds. Despite this, there is very little literature available on hysteresis in these systems. Most studies examine only the compression branch of the hysteresis loop, since the range of pressures over which the isotherms can be determined is limited to surface pressures below that at which the monolayer collapses and forms a three-dimensional multilayer system. The asymmetric shape of the hysteresis in the isotherms presented in Fig. 16 is, however, very similar to that found experimentally for certain temperatures and compression rates [see, for example, Fig. 3(b) of Ref. 44]. It is interesting to see that this asymmetry is reflected by almost symmetrical hysteresis in the plot of large-disk concentration as a function of area [Fig. 12(a)].

For the few experimental systems for which hysteresis has been reported, no discussion has been made of the phase structure around the hysteresis loop. However, in our simulations, we find that there are two intermediate phases observed for $\nu = 10^5$ as the system is compressed with increasing pressure from the low-density fluid phase to the high-density solid phase. The first of these phases is characterized by chain conformational disorder and positional order (that is, a large-disk solid in the language of the minimal model), and the second is characterized by chain conformational order and positional disorder (a small-disk liquid). As the system is expanded with decreasing pressure, only the second of these is observed as a distinct intermediate phase. This indicates that hysteresis can be associated with a rich phase behavior in systems such as lipid monolayers.

It should be pointed out that there is a close thermodynamic relationship[41] between pressure-induced transitions in lipid monolayers and thermally driven transitions in fully hydrated lipid bilayers. Hence the models presented in this paper may also provide a new approach for studying the phase behavior of bilayers at constant pressure. In the bilayer systems, the acyl-chain conformational ordering transition and the crystallization process are believed to occur simultaneously in equilibrium,[51–53] although they may decouple out of equilibrium or due to the presence of a suitable second component such as choloesterol.[29]

The models proposed in the present paper hold a promise for advances in the theoretical modeling of lipid systems. This not only applies to pure systems but also to lipid systems with other molecular components in fixed concentration, specifically molecules like proteins, cholesterol, and anesthetics, for which the packing properties in the lipid layer are very important for the phase behavior and ultimately for membrane function.

ACKNOWLEDGMENTS

This work was supported by the Natural Sciences and Engineering Research Council of Canada, by Fonds pour la formation de Chercheurs et l'Aide á la Recherche du Québec, and by the Danish Natural Science Research Council under Grant J.nr. 5219971. Diane Fraser's work in Denmark was supported by the Danish Natural Science Research Council under Grant J.nr. 11-7785, and Martin Zuckermann's work in Denmark was supported by the Danish Research Academy under Grant J.nr. F890095. Stimulating discussions with Bruce Lennox regarding hysteresis in lipid monolayers are gratefully acknowledged.

[1]E. Helfand, H. L. Frisch, and J. L. Lebowitz, J. Chem. Phys. **34**, 1037 (1961).
[2]J. L. Lebowitz, E. Helfand, and E. Praestgaard, J. Chem. Phys. **43**, 774 (1965).
[3]M. A. Cotter and F. H. Stillinger, J. Chem. Phys. **57**, 3356 (1972).
[4]D. Henderson, Mol. Phys. **30**, 971 (1975).
[5]F. Lado, J. Chem. Phys. **49**, 3092 (1968).
[6]F. C. Andrews, J. Chem. Phys. **64**, 1941 (1976).
[7]See, for example, J. P. Hansen and I. R. MacDonald, *Theory of Simple Liquids* (Academic, New York, 1976). Note that the 2nd edition (1986) omits any reference to two-dimensional systems.
[8]T. Boublík, Mol. Phys. **29**, 421 (1975).
[9]R. Tenne and E. Bergmann, J. Chem. Phys. **70**, 1952 (1979).
[10]J. Talbot and D. J. Tildesley, J. Chem. Phys. **83**, 6419 (1985).
[11]R. J. Bearman and R. M. Mazo, J. Chem. Phys. **88**, 1235 (1988).
[12]D. A. Ward and F. Lado, Mol. Phys. **63**, 623 (1988).
[13]T. Boublík, Mol. Phys. **63**, 685 (1988).
[14]D. A. Ward and F. Lado, Mol. Phys. **64**, 1185 (1988).
[15]Y. Song and E. A. Mason, J. Chem. Phys. **93**, 686 (1990).

[16]H. L. Scott and W. H. Cheng, Biophys. J. **28**, 117 (1979).
[17]D. A. Kofke and E. D. Glandt, J. Chem. Phys. **87**, 4881 (1987).
[18]M. R. Stapleton, D. J. Tildesley, T. J. Sluckin, and N. Quirke, J. Phys. Chem. **92**, 4788 (1988).
[19]D. P. Fraser, R. W. Chantrell, D. Melville, and D. J. Tildesley, Liquid Crystals **3**, 423 (1988).
[20]D. A. Kofke and E. D. Glandt, J. Chem. Phys. **90**, 439 (1989).
[21]M. R. Stapelton and A. Z. Panagiotopoulos, J. Chem. Phys. **92**, 1285 (1990).
[22]J. N. Israelachvili, D. J. Mitchell, and B. W. Ninham, J. Chem. Soc. Faraday Trans. 2 **72**, 1525 (1976).
[23]P. J. Quinn and D. Chapman, CRC Crit. Rev. Biochem. **8**, 1 (1980).
[24]O. G. Mouritsen, in *Physics in Living Matter,* edited by D. Baeriswyl, M. Droz, A. Malaspinas, and P. Martinoli (Springer-Verlag, Berlin 1987), Vol. 284, Chap. III, p. 76.
[25]S. H. Northrup and M. S. Curvin, J. Phys. Chem. **89**, 4707 (1985).
[26]J. P. Bareman, G. Cardini, and M. L. Klein, Phys. Rev. Lett. **60**, 2152 (1988).
[27]J. Harris and S. A. Rice, J. Chem. Phys. **89**, 5898 (1988).
[28]O. G. Mouritsen and M. J. Zuckermann, Chem. Phys. Lett. **135**, 294 (1987).
[29]J. H. Ipsen, O. G. Mouritsen, and M. J. Zuckermann, J. Chem. Phys. **91**, 1855 (1989).
[30]P. J. Flory, *Principles of Polymer Chemistry* (Cornell University, Ithaca, 1953), Chap. X.
[31]P. Tevlin, F. P. Jones, and L. E. H. Trainor, J. Chem. Phys. **87**, 5483 (1987).
[32]S. Doniach, J. Chem. Phys. **68**, 4912 (1978).
[33]A. Caillé, D. A. Pink, F. de Verteuil, and M. J. Zuckermann, Can. J. Phys. **58**, 581 (1980).
[34]D. A. Pink, T. J. Green, and D. Chapman, Biochem. **19**, 349 (1980).
[35]F. P. Jones, P. Tevlin, and L. E. H. Trainor, J. Chem. Phys. **91**, 1918 (1989).
[36]F. P. Jones, Ph.D. thesis, University of Toronto, 1991.
[37]D. P. Fraser, M. J. Zuckermann, and O. G. Mouritsen, Phys. Rev. A **42**, 3186 (1990).
[38]F. P. Preparata and M. I. Shamos, *Computational Geometry, An Introduction* (Springer-Verlag, Berlin, 1985).
[39]E. Helfand, H. Reiss, H. L. Frisch, and J. L. Lebowitz, J. Chem. Phys. **33**, 1379 (1960).
[40]E. D. Specht, A. Mak, C. Peters, M. Sutton, R. J. Birgeneau, K. L. d'Amico, D. E. Moncton, S. E. Nagler, and P. M. Horn, Z. Phys. B **69**, 347 (1987).
[41]O. Albrecht, H. Gruler, and E. Sackmann, J. Phys. (Paris) **39**, 301 (1978).
[42]W. D. Harkins and E. Boyd, J. Phys. Chem. **45**, 20 (1941).
[43]M. C. Phillips and D. Chapman, Biochem. Biophys. Acta **163**, 301 (1968).
[44]H. -D. Dörfler and W. Rettig, Colloid Polymer Sci. **258**, 415 (1980).
[45]G. M. Bell, L. L. Combs, and L. J. Dunne, Chem. Rev. **81**, 15 (1981).
[46]V. von Tscharner and H. M. McConnell, Biophys. J. **36**, 409 (1981).
[47]J. Mingins, J. A. G. Taylor, B. A. Pethica, C. M. Jackson, and B. Y. T. Yue, J. Chem. Soc. Faraday Trans. 1 **78**, 323 (1982).
[48]J. F. Nagle, Ann. Rev. Phys. Chem. **31**, 157 (1980).
[49]I. Jalal and G. Zografi, J. Colloid Interface Sci. **68**, 196 (1979).
[50]D. A. Cadenhead, in *Structure of Biological Membranes,* edited by S. Abrahamsson and I. Pascher (Plenum, New York, 1977), p. 63.
[51]M. Caffrey, Biochem. **24**, 4826 (1985).
[52]O. G. Mouritsen and M. J. Zuckermann, Phys. Rev. Lett. **58**, 389 (1987).
[53]M. J. Zuckermann and O. G. Mouritsen, Eur. Biophys. J. **15**, 77 (1987).